Color Invariance

Jan-Mark Geusebroek, Rein van den Boomgaard, *Member*, *IEEE Computer Society*, Arnold W.M. Smeulders, *Senior Member*, *IEEE*, and Hugo Geerts

Abstract—This paper presents the measurement of colored object reflectance, under different, general assumptions regarding the imaging conditions. We exploit the Gaussian scale-space paradigm for color images to define a framework for the robust measurement of object reflectance from color images. Object reflectance is derived from a physical reflectance model based on the Kubelka-Munk theory for colorant layers. Illumination and geometrical invariant properties are derived from the reflectance model. Invariance and discriminative power of the color invariants is experimentally investigated, showing the invariants to be successful in discounting shadow, illumination, highlights, and noise. Extensive experiments show the different invariants to be highly discriminative, while maintaining invariance properties. The presented framework for color measurement is well-founded in the physics of color as well as in measurement science. Hence, the proposed invariants are considered more adequate for the measurement of invariant color features than existing methods.

Index Terms—Photometric invariance, color constancy, measurement theory, scale-space, differential invariants, differential geometry, multispectral imaging, Kubelka-Munk theory, photometric models, Gaussian color model.

1 Introduction

It is well-known that color is a powerful cue in the distinction and recognition of objects. Segmentation based on color, rather than just intensity, provides a broader class of discrimination between material boundaries. Modeling the physical process of color image formation provides a clue to the object-specific parameters [1], [2], [3], [4]. To reduce some of the complexity intrinsic to color images, parameters with known invariance are of prime importance. Current methods for the measurement of color invariance require a fully sampled spectrum as input data usually derived by a spectrometer. Angelopoulou et al. [5] use the spectral gradient to estimate surface reflectance from multiple images of the same scene, captured with different spectral narrow band filters. The assumptions underlying their approach require a smoothly varying illumination. Their method is able to accurately estimate surface reflectance independent of the scene geometry. Stokman and Gevers [6] propose a method for edge classification from spectral images. Their method aims in detecting edges and assigning one of the types; shadow or geometry, highlight, or a material edge. Under the assumption of spectral narrow band filters, and for a known illumination spectrum, they prove their method to be accurate in edge classification. These approaches hampers broad use as spectrometers are both slow and expensive. In addition, they do not provide two-dimensional spatial resolution easily. In this paper, we aim at a broad range of color invariants measured from RGB-cameras.

To that end, differential geometry is adopted as the framework for feature detection and segmentation of images. Its impact in computer vision is overwhelming but mostly limited to gray-value images [7], [8], [9]. Embedding the theory in the scale-space paradigm [10], [11] resulted in well-posed differential operators robust against noisy measurements, with the Gaussian aperture as the fundamental operator. Only a few papers are available on color differential geometry [12], [13], which are mainly based on the color gradient proposed by Di Zenzo [14]. In the paper, an expression for the color gradient is derived by analysis of the eigensystem of the color structure tensor. In [15], curvature and zero-crossing detection is investigated for the directional derivative of the color gradient. For these geometrical invariants no physical model is taken into account, yielding measurements which are highly influenced by the specific imaging circumstances as shadow, illumination, and viewpoint. We consider the introduction of wavelength in the scale-space paradigm, as suggested by Koenderink and Kappers [16]. This leads to a spatio-spectral family of Gaussian aperture functions, in [17] as the Gaussian color model. Hence, the Gaussian color model may be considered an extension of the differential geometry framework into the spatio-spectral domain. In the paper we apply the spatio-spectral scale-space to the measurement of photometric and geometric invariants.

In [18], [19], the authors discuss the use of the Shafer model [4], effectively based on the older Kubelka-Munk theory [20], to measure object reflectance independent of illumination color. The Kubelka-Munk theory models the reflected spectrum of a colored body [21], [22], based on a material-dependent scattering and absorption function, under the assumption that light is isotropically scattered within the material. The theory has proven to be successful for a wide

- *J.-M. Geusebroek, R. van den Boomgaard, and A.W.M. Smeulders are with Intelligent Senorsory Information Systems, Department of Computer Science, Faculty of Science, University of Amsterdam, Kruislaan 403, 1098 SJ Amsterdam, The Netherlands.*
  E-mail: {geusebroek, rein, smeulders}@science.uva.nl.
- *H. Geerts is with Neurobiology, CNS Discovery Research, Janssen Research Foundation, Turnhoutseweg 30, B2340 Beerse, Belgium.*
  E-mail: geusebroek@science.uva.nl.

Manuscript received 4 Jan. 2000; revised 12 Dec. 2000; accepted 4 May 2001. Recommended for acceptance by S. Sarkar.
For information on obtaining reprints of this article, please send e-mail to: tpami@computer.org, and reference IEEECS Log Number 111164.

variety of materials and applications [21]. Therefore, the Kubelka-Munk theory is well-suited for determining material properties from color measurements. We use the Kubelka-Munk theory for the definition of object reflectance properties, for a wide range of assumptions regarding imaging conditions.

The measurement of invariance involves a balance between constancy of the measurement regardless of the disturbing influence of the unwanted transform on the one hand, and retained discriminating power between truly different states of the objects on the other. As a general rule, features allowing ignorance of a larger set of disturbing factors, less discriminative power can be expected. We refer to such features as broad features. Hence, both invariance and discriminating power of a method should be investigated simultaneously. Only this allows to asses the practical performance of the proposed method. In this paper, we extensively investigate invariant properties and discriminative power.

The paper is organized as follows: Section 2 describes a physical model for image formation, based on the Kubelka-Munk theory. The first contribution of this paper is a complete set of invariant expressions derived for basically three different imaging conditions (Section 3). A second important contribution considers the robust measurement of invariant expressions from RGB-images (Section 4). Further, Section 4 demonstrates the performance of the features as invariance and discriminative power between different colored patches, which may be considered as a third contribution.

2 Color Image Formation Model

In [18], [19], [23], image formation is modeled by means of the Kubelka-Munk theory [21], [22], [24] for colorant layers. Under the assumption that light within the material is isotropically scattered, the material layer may be characterized by a wavelength dependent scatter coefficient and absorption coefficient. The model unites both reflectance of light and transparent materials. The class of materials for which the theory is useful ranges from dyed paper and textiles, opaque plastics, paint films, up to enamel, and dental silicate cements [21]. In the sequel, we will derive color invariant expressions under various imaging conditions. Therefore, an image formation model adequate for reflectance of light in real-world scenes is considered. We consider the Kubelka-Munk theory as a general model for color image formation. The photometric reflectance model resulting from the Kubelka-Munk theory is given by [19]

$$E(\lambda,\vec{x}) = e(\lambda,\vec{x})(1-\rho_{\mathrm{f}}(\vec{x}))^2 R_\infty(\lambda,\vec{x}) + e(\lambda,\vec{x})\rho_{\mathrm{f}}(\vec{x}), \quad (1)$$

where x denotes the position at the imaging plane and λ the wavelength. Further, $e(\lambda,\vec{x})$ denotes the illumination spectrum and $\rho_{\mathrm{f}}(\vec{x})$ the Fresnel reflectance at $\vec{x}$. The material reflectivity is denoted by $R_\infty(\lambda,\vec{x})$. The reflected spectrum in the viewing direction is given by $E(\lambda,\vec{x})$. The model is valid when the material is thick, i.e., not transparent nor translucent, and when the optical resolution is high enough to consider patches (the image pixels) to be locally planar. When redefining symbols

$$c_b(\lambda,\vec{x}) = e(\lambda,\vec{x})R_\infty(\lambda,\vec{x}), \quad c_i(\lambda,\vec{x}) = e(\lambda,\vec{x}),$$

$m_b(\vec{x}) = (1-\rho_{\mathrm{f}}(\vec{x}))^2$, and $m_i(\vec{x}) = \rho_{\mathrm{f}}(\vec{x})$, (1) reduces to

$$E(\lambda,\vec{x}) = m_b(\vec{x})c_b(\lambda,\vec{x}) + m_i(\vec{x})c_i(\lambda,\vec{x}), \quad (2)$$

which is the dichromatic reflection model by Shafer [4].

Concerning the Fresnel reflectance, the photometric model assumes a neutral interface at the surface patch. As discussed in [4], [22], deviations of ρ_{f} over the visible spectrum are small for commonly used materials, therefore, the Fresnel reflectance coefficient may be considered constant.

The following special case can be derived. For matte, dull surfaces, the Fresnel coefficient can be considered neglectable, $\rho_{\mathrm{f}}(\vec{x}) \approx 0$, for which $E(\lambda,\vec{x})$ (1) reduces to the Lambertian model for diffuse body reflection

$$E(\lambda,\vec{x}) = e(\lambda,\vec{x})R_\infty(\lambda,\vec{x}), \quad (3)$$

as expected.

3 Determination of Color Invariants

Any method for finding invariant color properties relies on a photometric model and on assumptions about the physical variables involved. For example, hue is known to be insensitive to surface orientation, illumination direction, intensity and highlights, under an equal energy illumination [2]. Normalized rgb is an object property but only for matte, dull surfaces and only when illuminated by an equal energy spectrum. When the illumination color is not "white," other object properties should be measured.

In this section, expressions for determining invariant properties in color images will be derived for three different imaging conditions, taking into account the photometric model derived in Section 2. The imaging conditions are assumed to be the five relevant out of eight combinations of:

1. equal energy or arbitrary illumination,
2. matte, dull object or general object, or
3. uniformly stained object or generally colored object.

Further specialization as spatially uniform, hence, even illumination or a single illumination spectrum may be considered. Note that each essentially different condition of the scene, object or recording circumstances results in suited different invariant expressions. For notational convenience, we first concentrate on the one dimensional case; two-dimensional expressions will be derived later when introducing geometrical invariants.

3.1 Invariants for Equal Energy but Uneven Illumination

Consider the photometric reflection model (1). For an equal energy illumination, the spectral components of the source are constant over the wavelengths. Hence, a spatial component $i(x)$ denotes intensity variations, resulting in

$$E(\lambda,x) = i(x)\Big\{\rho_{\mathrm{f}}(x) + (1-\rho_{\mathrm{f}}(x))^2 R_\infty(\lambda,x)\Big\}. \quad (4)$$

The assumption allows the extraction of expressions describing object reflectance independent of the Fresnel reflectance. Let indices of λ and x indicate differentiation,

and from now on dropping (λ, x) from $E(\lambda, x)$ when such will cause no confusion.

Lemma 1. *Within the Kubelka-Munk model, assuming dichromatic reflection and equal energy illumination, $H = \frac{E_\lambda}{E_{\lambda\lambda}}$ is an object reflectance property independent of viewpoint, surface orientation, illumination direction, illumination intensity and Fresnel reflectance coefficient.*

Proof. Differentiating (4) with respect to λ twice results in

$$E_\lambda = i(x)(1-\rho_f(x))^2 \frac{\partial R_\infty(\lambda, x)}{\partial \lambda}$$

and

$$E_{\lambda\lambda} = i(x)(1-\rho_f(x))^2 \frac{\partial^2 R_\infty(\lambda, x)}{\partial \lambda^2}.$$

Hence, their ratio depends on derivatives of the object reflectance functions $R_\infty(\lambda, x)$ only, which proves the lemma. □

To interpret H, consider the local Taylor expansion at λ_0 truncated at second order,

$$E(\lambda_0 + \Delta\lambda) \approx E(\lambda_0) + \Delta\lambda E_\lambda(\lambda_0) + \frac{1}{2}\Delta\lambda^2 E_{\lambda\lambda}(\lambda_0). \quad (5)$$

The function extremum of $E_\lambda(\lambda_0 + \Delta\lambda)$ is at $\Delta\lambda$ for which the first order derivative is zero,

$$\frac{d}{d\lambda}\{E(\lambda_0 + \Delta\lambda)\} = E_\lambda(\lambda_0) + \Delta\lambda E_{\lambda\lambda}(\lambda_0) = 0. \quad (6)$$

Hence, for $\Delta\lambda$ near the origin λ_0,

$$\Delta\lambda_{\max} = -\frac{E_\lambda(\lambda_0)}{E_{\lambda\lambda}(\lambda_0)}. \quad (7)$$

In conclusion, the property H is related to the *hue* (i.e., $\arctan(\lambda_{max})$) of the material. For $E_{\lambda\lambda}(\lambda_0) < 0$ the result is at a maximum and describes a band-pass (prism) color, whereas for $E_{\lambda\lambda}(\lambda_0) > 0$ the result is at a minimum and indicates a band-stop (slit) color.

Of significant importance is the derivation of a complete set Ψ of functionally independent (irreducible) differential invariants Ψ_i. Completeness states that all possible independent invariants for the unwanted distortion are present in the set Ψ. From Olver et al. [25], the basic method for constructing a complete set of differential invariants is to use invariant differential operators. A differential operator is said to be invariant under a given distortion if it maps differential invariants to higher order differential invariants. Hence, by iteration, such an operator produces a hierarchy of differential invariants of arbitrarily large order n, given a lowest order invariant. The lowest order invariant is referred to as the fundamental invariant. Summarizing, for a lowest order color invariant, a differential operator may be defined to construct complete, irreducible sets of color invariants under the same imaging conditions by iteration.

Proposition 2. *A complete and irreducible set of color invariants, up to a given differential order, is given by all derivatives of the fundamental color invariant.*

In the sequel, we will define the generating differential operator given the lowest order fundamental invariant.

The expression given by Lemma 1 is a fundamental lowest order invariant. As a result of Proposition 2, differentiation of the expression for H with respect to x or λ results in object reflectance properties under an equal energy illumination. Note that H is ill-defined when the second order spectral derivative vanishes. We prefer to compute differentials of the $\arctan(H)$ a monotonic function of H, for which the spatial derivatives yield better numerical stability.

Corollary 3. *Within the Kubelka-Munk model, a complete and irreducible set of invariants for dichromatic reflection and an equal energy illumination is given by*

$$H_{\lambda^m x^n} = \frac{\partial^{m+n}}{\partial \lambda^m \partial x^n}\left\{\arctan\left(\frac{E_\lambda}{E_{\lambda\lambda}}\right)\right\}, \quad (8)$$

for $m, n \geq 0$.

Application of the chain rule for differentiation yields the higher order expressions in terms of the spatio-spectral energy distribution. For illustration, we give all expressions for first spatial derivative and second spectral order. The hue spatial derivative is given by

$$H_x = \frac{E_{\lambda\lambda}E_{\lambda x} - E_\lambda E_{\lambda\lambda x}}{E_\lambda^2 + E_{\lambda\lambda}^2} \quad (9)$$

admissible for $E_\lambda^2 + E_{\lambda\lambda}^2 > 0$.

In the sequel, we also need an expression for color saturation S,

$$S = \frac{1}{E(\lambda, x)}\sqrt{{E_\lambda}^2 + {E_{\lambda\lambda}}^2}. \quad (10)$$

3.2 Invariants for Equal Energy but Uneven Illumination and Matte, Dull Surfaces

A class of tighter invariants may be derived when the object is matte and dull. Consider the photometric reflection model (4), for matte, dull surfaces with low Fresnel reflectance, $\rho_f(\vec{x}) \approx 0$,

$$E = i(x)R_\infty(\lambda, x). \quad (11)$$

These assumptions allow the derivation of expressions describing object reflectance independent of the intensity distribution.

Lemma 4. *Within the Kubelka-Munk model, assuming matte, dull surfaces, and an equal energy illumination, $C_\lambda = \frac{E_\lambda}{E}$ is an object reflectance property independent of the viewpoint, surface orientation, illumination direction and illumination intensity.*

Proof. Differentiation of (11) with respect to λ and normalization by (11) results in an equation depending on object property only, $\frac{E_\lambda}{E} = \frac{1}{R_\infty(\lambda,x)}\frac{\partial R_\infty(\lambda,x)}{\partial \lambda}$ which proves the lemma. □

The property C_λ may be interpreted as describing object color regardless intensity.

As a result of Proposition 2, all normalized higher order spectral derivatives of C_λ, and their spatial derivatives,

result in object reflectance properties under an equal energy illumination. The normalization by E is to be evaluated at the spectral wavelength of interest and, therefore, is considered locally constant with respect to λ.

Corollary 5. *Within the Kubelka-Munk model, a complete and irreducible set of invariants for matte, dull surfaces, under an equal energy illumination is given by*

$$C_{\lambda^m x^n} = \frac{\partial^n}{\partial x^n}\left\{\frac{E_{\lambda^m}}{E}\right\}, \tag{12}$$

for $m \geq 1$, $n \geq 0$.

Specific first spatial and second spectral order expressions are given by

$$C_{\lambda\lambda} = \frac{E_{\lambda\lambda}}{E}, C_{\lambda x} = \frac{E_{\lambda x}E - E_\lambda E_x}{E^2}, C_{\lambda\lambda x} = \frac{E_{\lambda\lambda x}E - E_{\lambda\lambda}E_x}{E^2}. \tag{13}$$

Note that these expressions are valid everywhere $E > 0$. These invariants may be interpreted as the spatial derivative of the intensity normalized spectral slope C_λ and curvature $C_{\lambda\lambda}$.

3.3 Invariants for Equal Energy and Uniform Illumination and Matte, Dull Surfaces, and Planar Objects

For uniform illumination, consider again the photometric reflection model (11) for matte, dull surfaces, and an equal energy and uniform illumination with intensity i,

$$E(\lambda, x) = iR_\infty(\lambda, x). \tag{14}$$

The assumptions yield a Mondrian world, which may be achieved under well-defined circumstances, such as photography of art. These assumptions allow the derivation of expressions describing object reflectance independent of the intensity level.

Lemma 6. *Within the Kubelka-Munk model, assuming matte, dull surfaces, planar objects, and an equal energy and uniform illumination, $W_x = \frac{E_x}{E}$ determines changes in object reflectance independent of the illumination intensity.*

Proof. Differentiation of (14) with respect to x and normalization by (14) results in $\frac{E_x}{E} = \frac{1}{R_\infty(\lambda,x)}\frac{\partial R_\infty(\lambda,x)}{\partial x}$. This is an object reflectance property. □

The property W_x may be interpreted as an edge detector specific for changes in spectral distribution. Under common circumstances, a geometry dependent intensity term is present, hence W_x does not represent pure object properties but will include shadow edges where present.

As a result from Proposition 2, all normalized higher order derivatives of W_x yield object reflectance properties under an equal energy and uniform illumination. The normalization by E is to be evaluated at the spatial and spectral point of interest. Hence, it is considered locally constant.

Corollary 7. *Within the Kubelka-Munk model, a complete and irreducible set of invariants for matte, dull surfaces, planar objects, under an equal energy and uniform illumination is given by*

$$W_{\lambda^m x^n} = \frac{E_{\lambda^m x^n}}{E} \tag{15}$$

for $m \geq 0$, $n \geq 1$.

Specific expressions for $E > 0$ up to first spatial and second spectral order are given by

$$W_{\lambda x} = \frac{E_{\lambda x}}{E}, W_{\lambda\lambda x} = \frac{E_{\lambda\lambda x}}{E}. \tag{16}$$

These invariants may be interpreted as the intensity normalized spatial derivatives of the spectral intensity E, spectral slope E_λ and spectral curvature $E_{\lambda\lambda}$.

3.4 Invariants for Colored but Uneven Illumination

For colored illumination, when the spectral energy distribution of the illumination does not vary over the scene, the illumination may be decomposed into a spectral component $e(\lambda)$ representing the illumination color, and a spatial component $i(x)$ denoting variations in intensity due to the scene geometry. Hence, for matte, dull surfaces $\rho_f \to 0$,

$$E = e(\lambda)i(x)R_\infty(\lambda, x). \tag{17}$$

The assumption allows us to derive expressions describing object reflectance independent of the illumination.

Lemma 8 *Within the Kubelka-Munk model, assuming matte, dull surfaces and a single illumination spectrum, $N_{\lambda x} = \frac{E_{\lambda x}E - E_\lambda E_x}{E^2}$ determines changes in object reflectance independent of the viewpoint, surface orientation, illumination direction, illumination intensity, and illumination color.*

Proof. Differentiation of (17) with respect to λ results in

$$E_\lambda = i(x)R_\infty(\lambda, x)\frac{\partial e(\lambda)}{\partial \lambda} + e(\lambda)i(x)\frac{\partial R_\infty(\lambda, x)}{\partial \lambda}.$$

Dividing by (17) gives the relative differential,

$$\frac{E_\lambda}{E} = \frac{1}{e(\lambda)}\frac{\partial e(\lambda)}{\partial \lambda} + \frac{1}{R_\infty(\lambda, x)}\frac{\partial R_\infty(\lambda, x)}{\partial \lambda}.$$

The result consists of two terms, the former depending on the illumination color only and the latter depending on body and Fresnel reflectance only. Differentiation to x yields

$$\frac{\partial}{\partial x}\left\{\frac{E_\lambda}{E}\right\} = \frac{\partial}{\partial x}\left\{\frac{1}{R_\infty(\lambda, x)}\frac{\partial R_\infty(\lambda, x)}{\partial \lambda}\right\}.$$

The right-hand side is depending only on object property. This proves the lemma. □

The invariant $N_{\lambda x}$ may be interpreted as the spatial derivative of the spectral change of the reflectance function $R_\infty(\lambda, x)$ and, therefore, indicates transitions in object reflectance. Hence, $N_{\lambda x}$ determines material transitions regardless illumination color and intensity distribution.

As a result of Proposition 2, further differentiation of $N_{\lambda x}$ results in object reflectance properties under a colored illumination.

TABLE 1
Summary of the Various Color Invariant Sets and Their Invariance to Specific Imaging Conditions

	viewing direction	surface orientation	highlights	illumination direction	illumination intensity	illumination color	inter reflection
H	+	+	+	+	+	–	–
N	+	+	–	+	+	+	–
U	+	+	–	+	+	+	–
C	+	+	–	+	+	–	–
W	–	–	–	–	+	–	–
E	–	–	–	–	–	–	–

Invariance is denoted by +, whereas sensitivity to the imaging condition is indicated by –. Note that the reflected spectral energy distribution E is sensitive to all the conditions cited.

Corollary 9. *Within the Kubelka-Munk model, a complete and irreducible set of invariants for matte, dull surfaces, and a single illumination spectrum, is given by*

$$N_{\lambda^m x^n} = \frac{\partial^{m+n-2}}{\partial \lambda^{m-1} \partial x^{n-1}} \left\{ \frac{E_{\lambda x} E - E_\lambda E_x}{E^2} \right\}, \tag{18}$$

for $m \geq 1$, $n \geq 1$.

The third order example is the spectral derivative of $N_{\lambda x}$ for $E(\lambda, x) > 0$,

$$N_{\lambda\lambda x} = \frac{E_{\lambda\lambda x} E^2 - E_{\lambda\lambda} E_x E - 2E_{\lambda x} E_\lambda E + 2E_\lambda^2 E_x}{E^3}. \tag{19}$$

3.5 Invariants for a Uniform Object

For uniformly colored planar surface, the reflectance properties are spatially constant. Hence, the reflectance function R_∞ and Fresnel coefficient ρ_{f} are independent of x,

$$E = e(\lambda, x) \Big\{ \rho_{\mathrm{f}} + (1 - \rho_{\mathrm{f}})^2 R_\infty(\lambda) \Big\}. \tag{20}$$

For a single illumination source, expressions describing interreflections may be extracted, i.e., the reflected spectrum of surrounding materials.

Lemma 10. *Within the Kubelka-Munk model, assuming dichromatic reflection, a single illumination source, and a uniformly colored planar surface, $U_{\lambda x} = \frac{E_{\lambda x} E - E_\lambda E_x}{E^2}$ determines interreflections of colored objects, independent of the object spectral reflectance function.*

Proof. Differentiating (20) to λ results in

$$E_\lambda = \left\{ \rho_{\mathrm{f}} + (1 - \rho_{\mathrm{f}})^2 R_\infty(\lambda) \right\} \frac{\partial e(\lambda, x)}{\partial \lambda} + e(\lambda, x)(1 - \rho_{\mathrm{f}})^2 \frac{\partial R_\infty(\lambda)}{\partial \lambda}.$$

Normalization by (20),

$$\frac{E_\lambda}{E} = \frac{1}{e(\lambda, x)} \frac{\partial e(\lambda, x)}{\partial \lambda} + \frac{(1 - \rho_{\mathrm{f}})^2}{\rho_{\mathrm{f}} + (1 - \rho_{\mathrm{f}})^2 R_\infty(\lambda)} \frac{\partial R_\infty(\lambda)}{\partial \lambda}.$$

Differentiation with respect to x results in

$$\frac{\partial}{\partial x} \left\{ \frac{E_\lambda}{E} \right\} = \frac{\partial}{\partial x} \left\{ \frac{1}{e(\lambda, x)} \frac{\partial e(\lambda, x)}{\partial \lambda} \right\},$$

which depends on the illumination only. Differentiation yields the lemma. □

The property $U_{\lambda x}$ may be interpreted as describing edges due to interreflections and specularities. When ambient illumination is present casting a different spectral distribution, the invariant describes shadow edges due to the combined ambient illumination and incident illumination.

Note that the expression for Lemma 10 is identical to the expression in Lemma 8. Consequently, changes in object reflectance cannot be distinguished from interreflections in single images. Further differentiation of $U_{\lambda x}$ yield interreflections when assuming a uniform colored planar surface. The result is identical to (19).

3.6 Summary of Color Invariants

In conclusion, within the Kubelka-Munk model, various sets of invariants are derived as summarized in Table 1. The class of materials for which the invariants are useful ranges from dyed paper and textiles, opaque plastics, paint films, up to enamel, and dental silicate cements [21]. The invariant sets may be ordered by broadness of invariance, where broader sets allow ignorance of a larger set of disturbing factors than tighter sets.

The table offers the solution of using the narrowest set of invariants for known imaging conditions, since

$$H \subset N = U \subset C \subset W \subset E.$$

In the case that recording circumstances are unknown the table offers a broad to narrow hierarchy. Hence, an incremental strategy of invariant feature extraction may be applied. Combination of invariants open up the way to edge type classification as suggested in [26]. The vanishing of edges for certain invariants indicate if their cause is shading, specular reflectance, or material boundaries.

3.7 Geometrical Color Invariants in Two Dimensions

So far, we have established color invariant descriptors, based on differentials in the spectral and the spatial domain in one spatial dimension. When applied in two dimensions, the result is depending on the orientation of the image content. In order to obtain meaningful image descriptions, it is crucial to derive descriptors which are invariant with respect to translation, rotation, and scaling. For the gray-value luminance L geometrical invariants are well established [7]. Translation and scale invariance is obtained by examining the (Gaussian) scale-space, which is a natural representation for investigating the scaling behavior of image features [10]. Florack et al. [7] extent

TABLE 2
Summary of the First Order Geometrical Invariants for the Various Color Invariant Sets

	$\frac{\partial}{\partial w}$
H	$H_w = \sqrt{H_x^2 + H_y^2}$ $= \frac{1}{E_\lambda^2 + E_{\lambda\lambda}^2} \sqrt{(E_{\lambda\lambda} E_{\lambda x} - E_\lambda E_{\lambda\lambda x})^2 + (E_{\lambda\lambda} E_{\lambda y} - E_\lambda E_{\lambda\lambda y})^2}$
C_λ	$C_{\lambda w} = \sqrt{C_{\lambda x}^2 + C_{\lambda y}^2}$ $= \frac{1}{E^2} \sqrt{(E_{\lambda x} E - E_\lambda E_x)^2 + (E_{\lambda y} E - E_\lambda E_y)^2}$
$C_{\lambda\lambda}$	$C_{\lambda\lambda w} = \sqrt{C_{\lambda\lambda x}^2 + C_{\lambda\lambda y}^2}$ $= \frac{1}{E^2} \sqrt{(E_{\lambda\lambda x} E - E_{\lambda\lambda} E_x)^2 + (E_{\lambda\lambda y} E - E_{\lambda\lambda} E_y)^2}$
W	$I_w = \sqrt{W_x^2 + W_y^2}$ $= \frac{1}{E} \sqrt{E_x^2 + E_y^2}$
W_λ	$W_{\lambda w} = \sqrt{W_{\lambda x}^2 + W_{\lambda y}^2}$ $= \frac{1}{E} \sqrt{E_{\lambda x}^2 + E_{\lambda y}^2}$
$W_{\lambda\lambda}$	$W_{\lambda\lambda w} = \sqrt{W_{\lambda\lambda x}^2 + W_{\lambda\lambda y}^2}$ $= \frac{1}{E} \sqrt{E_{\lambda\lambda x}^2 + E_{\lambda\lambda y}^2}$
N_λ	$N_{\lambda w} = \sqrt{N_{\lambda x}^2 + N_{\lambda y}^2}$ $= \frac{1}{E^2} \sqrt{(E_{\lambda x} E - E_\lambda E_x)^2 + (E_{\lambda y} E - E_\lambda E_y)^2}$
$N_{\lambda\lambda}$	$N_{\lambda\lambda w} = \sqrt{N_{\lambda\lambda x}^2 + N_{\lambda\lambda y}^2}$ $= \frac{1}{E^3} \sqrt{(E_{\lambda\lambda x} E^2 - E_{\lambda\lambda} E_x E - 2E_{\lambda x} E_\lambda E + 2E_\lambda^2 E_x)^2 + (E_{\lambda\lambda y} E^2 - E_{\lambda\lambda} E_y E - 2E_{\lambda y} E_\lambda E + 2E_\lambda^2 E_y)^2}$

See Table 1 for invariant class.

the Gaussian scale-space with rotation invariance, by considering in a systematic manner local gauge coordinates. The coordinate axis w and v are aligned to the gradient and isophote tangents directions, respectively. Hence, the first order gradient gauge invariant is the magnitude of the luminance gradient,

$$L_w = \sqrt{L_x^2 + L_y^2}. \tag{21}$$

Note that the first order isophote gauge invariant is zero by definition. The second order invariants are given by

$$L_{vv} = \frac{L_x^2 L_{yy} - 2L_x L_y L_{xy} + L_y^2 L_{xx}}{L_w^2}, \tag{22}$$

related to isophote curvature,

$$L_{vw} = \frac{L_x L_y (L_{yy} - L_{xx}) - \left(L_x^2 - L_y^2\right) L_{xy}}{L_w^2} \tag{23}$$

related to flow-line curvature, and

$$L_{ww} = \frac{L_x^2 L_{xx} + 2L_x L_y L_{xy} + L_y^2 L_{yy}}{L_w^2} \tag{24}$$

related to isophote density. These spatial results may be combined with the color invariants for the 1D-case established before. The resulting first order expressions are given in Table 2.

Two or three measures for edge strength are derived, one for each spectral differential order. The only exception is H. Total edge strength due to differences in the energy distribution may be defined by the root squared sum of the edge strengths under a given imaging condition. A summary of total edge strength measures, ordered by degree of invariance, is given in Table 3.

For completeness, spatial second order derivatives in two dimensions are given in Tables 4 and 5. The derivation of higher order invariants is straightforward. Usually many derivatives are involved here, raising some doubt on the sustainable computational accuracy of the result.

4 Measurement of Color Invariants

4.1 The Gaussian Color Model

Up to this point we have considered invariant expressions describing material properties under some general assumptions. They are derived from expressions exploring the infinitely dimensional Hilbert space of spectra at an infinitesimally small spatial neighborhood. In practice, the spatio-spectral energy distribution is measurable only at a certain spatial extend and a certain spectral bandwidth.

TABLE 3
Summary of the Total Edge Strength Measures for the Various Color Invariant Sets, Ordered by Degree of Invariance

E	$E_w = \sqrt{E_x^2 + E_{\lambda x}^2 + E_{\lambda\lambda x}^2 + E_y^2 + E_{\lambda y}^2 + E_{\lambda\lambda y}^2}$
W	$W_w = \sqrt{W_x^2 + W_{\lambda x}^2 + W_{\lambda\lambda x}^2 + W_y^2 + W_{\lambda y}^2 + W_{\lambda\lambda y}^2}$
C	$C_w = \sqrt{C_{\lambda x}^2 + C_{\lambda\lambda x}^2 + C_{\lambda y}^2 + C_{\lambda\lambda y}^2}$
N	$N_w = \sqrt{N_{\lambda x}^2 + N_{\lambda\lambda x}^2 + N_{\lambda y}^2 + N_{\lambda\lambda y}^2}$
H	$H_w = \sqrt{H_x^2 + H_y^2}$

The edge strength E_w is not invariant to any change in imaging conditions. See Table 1 for invariant class.

TABLE 4
Summary of the Spatial Second Order Derivatives for the Various Color Invariant Sets

	$\frac{\partial}{\partial x x}$	$\frac{\partial}{\partial x y}$
H	$H_{xx} = \frac{-2(E_{\lambda\lambda}E_{\lambda x} - E_\lambda E_{\lambda\lambda x})(E_\lambda E_{\lambda x} + E_{\lambda\lambda}E_{\lambda\lambda x})}{(E_\lambda^2 + E_{\lambda\lambda}^2)^2} + \frac{(E_\lambda^2 + E_{\lambda\lambda}^2)(E_{\lambda\lambda}E_{\lambda x x} - E_\lambda E_{\lambda\lambda x x})}{(E_\lambda^2 + E_{\lambda\lambda}^2)^2}$	$H_{xy} = \frac{-2(E_{\lambda\lambda}E_{\lambda x} - E_\lambda E_{\lambda\lambda x})(E_\lambda E_{\lambda y} + E_{\lambda\lambda}E_{\lambda\lambda y})}{(E_\lambda^2 + E_{\lambda\lambda}^2)^2} + \frac{(E_\lambda^2 + E_{\lambda\lambda}^2)(E_{\lambda\lambda}E_{\lambda x y} - E_\lambda E_{\lambda\lambda x y} - E_{\lambda y}E_{\lambda\lambda x} + E_{\lambda x}E_{\lambda\lambda y})}{(E_\lambda^2 + E_{\lambda\lambda}^2)^2}$
C_λ	$C_{\lambda x x} = \frac{E_{\lambda x x}E^2 - E_\lambda E_{x x}E - 2E_{\lambda x}E_x E + 2E_\lambda E_x^2}{E^3}$	$C_{\lambda x y} = \frac{E_{\lambda x y}E^2 + E_{\lambda x}E_y E - E_{\lambda y}E_x E - E_\lambda E_{x y}E - 2E_{\lambda x}E_y E + 2E_\lambda E_x E_y}{E^3}$
$C_{\lambda\lambda}$	$C_{\lambda\lambda x x} = \frac{E_{\lambda\lambda x x}E^2 - E_{\lambda\lambda}E_{x x}E - 2E_{\lambda\lambda x}E_x E + 2E_{\lambda\lambda}E_x^2}{E^3}$	$C_{\lambda\lambda x y} = \frac{E_{\lambda\lambda x y}E^2 + E_{\lambda\lambda x}E_y E - E_{\lambda\lambda y}E_x E - E_{\lambda\lambda}E_{x y}E - 2E_{\lambda\lambda x}E_y E + 2E_{\lambda\lambda}E_x E_y}{E^3}$
W	$W_{xx} = \frac{E_{xx}}{E}$	$W_{xy} = \frac{E_{xy}}{E}$
W_λ	$W_{\lambda xx} = \frac{E_{\lambda xx}}{E}$	$W_{\lambda xy} = \frac{E_{\lambda xy}}{E}$
$W_{\lambda\lambda}$	$W_{\lambda\lambda xx} = \frac{E_{\lambda\lambda xx}}{E}$	$W_{\lambda\lambda xy} = \frac{E_{\lambda\lambda xy}}{E}$
N_λ	$N_{\lambda xx} = \frac{E_{\lambda xx}E^2 - E_\lambda E_{xx}E - 2E_{\lambda x}E_x E + 2E_\lambda E_x^2}{E^3}$	$N_{\lambda xy} = \frac{E_{\lambda xy}E^2 + E_{\lambda x}E_y E - E_{\lambda y}E_x E - E_\lambda E_{xy}E - 2E_{\lambda x}E_y E + 2E_\lambda E_x E_y}{E^3}$
$N_{\lambda\lambda}$	$N_{\lambda\lambda xx} = \frac{E_{\lambda\lambda xx}E - E_{\lambda\lambda}E_{xx} - 2E_{\lambda xx}E_\lambda - 2E_{\lambda\lambda x}E_x - 2E_{\lambda x}^2}{E^2} + \frac{2E_{\lambda\lambda}E_x^2 E + 8E_{\lambda x}E_\lambda E_x E + 2E_\lambda^2 E_{xx}E - 6E_\lambda^2 E_x^2}{E^4}$	$N_{\lambda\lambda xy} = \frac{E_{\lambda\lambda xy}E - E_{\lambda\lambda}E_{xy} - 2E_{\lambda xy}E_\lambda - E_{\lambda\lambda x}E_y - E_{\lambda\lambda y}E_x - 2E_{\lambda x}E_{\lambda y}}{E^2} + \frac{2E_{\lambda\lambda}E_x E_y E + 4E_{\lambda x}E_\lambda E_y E + 4E_{\lambda y}E_\lambda E_x E + 2E_\lambda^2 E_{xy}E - 6E_\lambda^2 E_x E_y}{E^4}$

Hence, physical measurements imply integration over spectral and spatial dimensions. The integration reduces the infinitely dimensional Hilbert space of spectra at infinitesimally small spatial neighborhood to a limited amount of measurements. As suggested by Koenderink and Kappers [16], general aperture functions are to be used to probe the spatio-spectral energy distribution. In this section, we consider the Gaussian color model as a general model for the measurement of spatio-spectral differential quotients. In this section, no essentially new color model is proposed, but rather a theory of color measurement.

4.1.1 The Spectral Structure of Color

From scale space theory we know how to probe a function at a certain scale; the probe should have a Gaussian shape in order to prevent the creation of extra details into the function when observed at a higher scale (lower resolution) [10]. We consider the Gaussian as a general probe for the measurement of spatio-spectral differential quotients. We follow [17] for the Gaussian color model. Let $E(\lambda)$ be the energy distribution of the incident light, where λ denotes wavelength, and let $G(\lambda_0; \sigma_\lambda)$ be the Gaussian at spectral scale σ_λ positioned at λ_0. The spectral energy distribution may be approximated by a Taylor expansion at λ_0,

TABLE 5
Summary of the Second Order Geometrical Invariants for the Various Color Invariant Sets

	$\frac{\partial}{\partial v v}$	$\frac{\partial}{\partial v w}$	$\frac{\partial}{\partial w w}$
H	$H_{vv} = \frac{H_x^2 H_{yy} - 2H_x H_y H_{xy} + H_y^2 H_{xx}}{H_w^2}$	$H_{vw} = \frac{H_x H_y (H_{xx} - H_{yy}) - (H_x^2 - H_y^2) H_{xy}}{H_w^2}$	$H_{ww} = \frac{H_x^2 H_{xx} + 2H_x H_y H_{xy} + H_y^2 H_{yy}}{H_w^2}$
C_λ	$C_{\lambda vv} = \frac{C_{\lambda x}^2 C_{\lambda yy} - 2C_{\lambda x}C_{\lambda y}C_{\lambda xy}}{C_{\lambda w}^2} + \frac{C_{\lambda y}^2 C_{\lambda xx}}{C_{\lambda w}^2}$	$C_{\lambda vw} = \frac{C_{\lambda x}C_{\lambda y}(C_{\lambda xx} - C_{\lambda yy})}{C_{\lambda w}^2} - \frac{(C_{\lambda x}^2 - C_{\lambda y}^2)C_{\lambda xy}}{C_{\lambda w}^2}$	$C_{\lambda ww} = \frac{C_{\lambda x}^2 C_{\lambda xx} + 2C_{\lambda x}C_{\lambda y}C_{\lambda xy}}{C_{\lambda w}^2} + \frac{C_{\lambda y}^2 C_{\lambda yy}}{C_{\lambda w}^2}$
$C_{\lambda\lambda}$	$C_{\lambda\lambda vv} = \frac{C_{\lambda\lambda x}^2 C_{\lambda\lambda yy} - 2C_{\lambda\lambda x}C_{\lambda\lambda y}C_{\lambda\lambda xy}}{C_{\lambda\lambda w}^2} + \frac{C_{\lambda\lambda y}^2 C_{\lambda\lambda xx}}{C_{\lambda\lambda w}^2}$	$C_{\lambda\lambda vw} = \frac{C_{\lambda\lambda x}C_{\lambda\lambda y}(C_{\lambda\lambda xx} - C_{\lambda\lambda yy})}{C_{\lambda\lambda w}^2} - \frac{(C_{\lambda\lambda x}^2 - C_{\lambda\lambda y}^2)C_{\lambda\lambda xy}}{C_{\lambda\lambda w}^2}$	$C_{\lambda\lambda ww} = \frac{C_{\lambda\lambda x}^2 C_{\lambda\lambda xx} + 2C_{\lambda\lambda x}C_{\lambda\lambda y}C_{\lambda\lambda xy}}{C_{\lambda\lambda w}^2} + \frac{C_{\lambda\lambda y}^2 C_{\lambda\lambda yy}}{C_{\lambda\lambda w}^2}$
W	$I_{vv} = \frac{E_x^2 E_{yy} - 2E_x E_y E_{xy} + E_y^2 E_{xx}}{E\sqrt{E_x^2 + E_y^2}}$	$I_{vw} = \frac{E_x E_y (E_{xx} - E_{yy}) - (E_x^2 - E_y^2) E_{xy}}{E\sqrt{E_x^2 + E_y^2}}$	$I_{ww} = \frac{E_x^2 E_{xx} + 2E_x E_y E_{xy} + E_y^2 E_{yy}}{E\sqrt{E_x^2 + E_y^2}}$
W_λ	$W_{\lambda vv} = \frac{E_{\lambda x}^2 E_{\lambda yy} - 2E_{\lambda x}E_{\lambda y}E_{\lambda xy}}{E\sqrt{E_{\lambda x}^2 + E_{\lambda y}^2}} + \frac{E_{\lambda y}^2 E_{\lambda xx}}{E\sqrt{E_{\lambda x}^2 + E_{\lambda y}^2}}$	$W_{\lambda vw} = \frac{E_{\lambda x}E_{\lambda y}(E_{\lambda xx} - E_{\lambda yy})}{E\sqrt{E_{\lambda x}^2 + E_{\lambda y}^2}} - \frac{(E_{\lambda x}^2 - E_{\lambda y}^2)E_{\lambda xy}}{E\sqrt{E_{\lambda x}^2 + E_{\lambda y}^2}}$	$W_{\lambda ww} = \frac{E_{\lambda x}^2 E_{\lambda xx} + 2E_{\lambda x}E_{\lambda y}E_{\lambda xy}}{E\sqrt{E_{\lambda x}^2 + E_{\lambda y}^2}} + \frac{E_{\lambda y}^2 E_{\lambda yy}}{E\sqrt{E_{\lambda x}^2 + E_{\lambda y}^2}}$
$W_{\lambda\lambda}$	$W_{\lambda\lambda vv} = \frac{E_{\lambda\lambda x}^2 E_{\lambda\lambda yy} - 2E_{\lambda\lambda x}E_{\lambda\lambda y}E_{\lambda\lambda xy}}{E\sqrt{E_{\lambda\lambda x}^2 + E_{\lambda\lambda y}^2}} + \frac{E_{\lambda\lambda y}^2 E_{\lambda\lambda xx}}{E\sqrt{E_{\lambda\lambda x}^2 + E_{\lambda\lambda y}^2}}$	$W_{\lambda\lambda vw} = \frac{E_{\lambda\lambda x}E_{\lambda\lambda y}(E_{\lambda\lambda xx} - E_{\lambda\lambda yy})}{E\sqrt{E_{\lambda\lambda x}^2 + E_{\lambda\lambda y}^2}} - \frac{(E_{\lambda\lambda x}^2 - E_{\lambda\lambda y}^2)E_{\lambda\lambda xy}}{E\sqrt{E_{\lambda\lambda x}^2 + E_{\lambda\lambda y}^2}}$	$W_{\lambda\lambda ww} = \frac{E_{\lambda\lambda x}^2 E_{\lambda\lambda xx} + 2E_{\lambda\lambda x}E_{\lambda\lambda y}E_{\lambda\lambda xy}}{E\sqrt{E_{\lambda\lambda x}^2 + E_{\lambda\lambda y}^2}} + \frac{E_{\lambda\lambda y}^2 E_{\lambda\lambda yy}}{E\sqrt{E_{\lambda\lambda x}^2 + E_{\lambda\lambda y}^2}}$
N_λ	$N_{\lambda vv} = \frac{N_{\lambda x}^2 N_{\lambda yy} - 2N_{\lambda x}N_{\lambda y}N_{\lambda xy}}{N_{\lambda w}^2} + \frac{N_{\lambda y}^2 N_{\lambda xx}}{N_{\lambda w}^2}$	$N_{\lambda vw} = \frac{N_{\lambda x}N_{\lambda y}(N_{\lambda xx} - N_{\lambda yy})}{N_{\lambda w}^2} - \frac{(N_{\lambda x}^2 - N_{\lambda y}^2)N_{\lambda xy}}{N_{\lambda w}^2}$	$N_{\lambda ww} = \frac{N_{\lambda x}^2 N_{\lambda xx} + 2N_{\lambda x}N_{\lambda y}N_{\lambda xy}}{N_{\lambda w}^2} + \frac{N_{\lambda y}^2 N_{\lambda yy}}{N_{\lambda w}^2}$
$N_{\lambda\lambda}$	$N_{\lambda\lambda vv} = \frac{N_{\lambda\lambda x}^2 N_{\lambda\lambda yy} - 2N_{\lambda\lambda x}N_{\lambda\lambda y}N_{\lambda\lambda xy}}{N_{\lambda\lambda w}^2} + \frac{N_{\lambda\lambda y}^2 N_{\lambda\lambda xx}}{N_{\lambda\lambda w}^2}$	$N_{\lambda\lambda vw} = \frac{N_{\lambda\lambda x}N_{\lambda\lambda y}(N_{\lambda\lambda xx} - N_{\lambda\lambda yy})}{N_{\lambda\lambda w}^2} - \frac{(N_{\lambda\lambda x}^2 - N_{\lambda\lambda y}^2)N_{\lambda\lambda xy}}{N_{\lambda\lambda w}^2}$	$N_{\lambda\lambda ww} = \frac{N_{\lambda\lambda x}^2 N_{\lambda\lambda xx} + 2N_{\lambda\lambda x}N_{\lambda\lambda y}N_{\lambda\lambda xy}}{N_{\lambda\lambda w}^2} + \frac{N_{\lambda\lambda y}^2 N_{\lambda\lambda yy}}{N_{\lambda\lambda w}^2}$

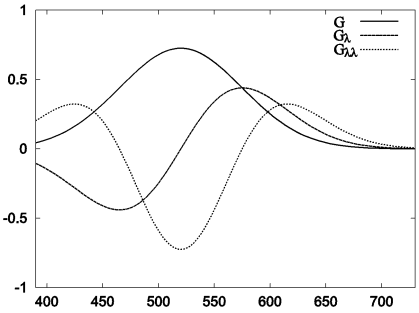

Fig. 1. The Gaussian sensitivity functions over the wavelengths. The incoming spectrum $E(\lambda)$ is weighted and integrated over the three sensitivity curves $\{G(\lambda;\lambda_0,\sigma_\lambda), G_\lambda(\lambda;\lambda_0,\sigma_\lambda), G_{\lambda\lambda}(\lambda;\lambda_0,\sigma_\lambda)\}$, yielding the three spectral measurements $\hat{E}$, $\hat{E}_\lambda$, and $\hat{E}_{\lambda\lambda}$. The Gaussian central wavelength $\lambda_0 = 520$ nm and scale $\sigma_\lambda = 55$ nm are chosen such that compatibility with human vision is achieved.

$$E(\lambda) = E^{\lambda_0} + \lambda E^{\lambda_0}_{\lambda} + \frac{1}{2}\lambda^2 E^{\lambda_0}_{\lambda\lambda} + \dots. \tag{25}$$

Measurement of the spectral energy distribution with a Gaussian aperture yields a weighted integration over the spectrum. The observed energy in the Gaussian color model $\hat{E}(\lambda)$, at infinitely small spatial resolution and spectral scale σ_λ, is in second order equal to [16]

$$\hat{E}^{\sigma_\lambda} = \hat{E}^{\lambda_0,^\sigma\lambda} + \lambda \hat{E}^{\lambda_0,\sigma_\lambda}_{\lambda} + \frac{1}{2}\lambda^2 \hat{E}^{\lambda_0,\sigma_\lambda}_{\lambda_\lambda} + O(\lambda^3), \tag{26}$$

where $\hat{E}^{\lambda_0,\sigma_\lambda} = \int E(\lambda)G(\lambda;\lambda_0,\sigma_\lambda)d\lambda$ measures the spectral intensity. Then, differentiation

$$\hat{E}^0_\lambda, \sigma_\lambda = \int E(\lambda)G_\lambda(\lambda;\lambda_0,\sigma_\lambda)d\lambda,$$

gives the first order spectral derivative and

$$\hat{E}^{\lambda_0,\sigma_\lambda}_{\lambda\lambda} = \int E(\lambda)G_{\lambda\lambda}(\lambda;\lambda_0,\sigma_\lambda)d\lambda,$$

measures the second order spectral derivative. The aperture functions G, G_λ, and $G_{\lambda\lambda}$ denote derivatives of the Gaussian with respect to λ, the sensitivities shown in Fig. 1. The model states that spectral measurement yields probing the differential structure of the spectrum. The measurements are obtained by integrating over the incoming spectrum, weighted by derived Gaussian sensitivity functions.

Definition 1 (Gaussian Color Model). *The Gaussian color model measures the coefficients $\hat{E}^{\lambda_0,\sigma_\lambda}$, $\hat{E}^{\lambda_0,\sigma_\lambda}_{\lambda}$, $\hat{E}^{\lambda_0,\sigma_\lambda}_{\lambda\lambda}$ ..., of the Taylor expansion of the Gaussian weighted spectral energy distribution at λ_0 and scale σ_λ.*

4.1.2 The Spatial Structure of Color

Introduction of spatial extent in the Gaussian color model yields a local Taylor expansion at wavelength λ_0 and position $\vec{x}_0$. Each measurement of a spatio-spectral energy distribution has a spatial as well as a spectral resolution. The measurement is obtained by probing an energy density volume in a three-dimensional spatio-spectral space. The size of the probe is determined by the observation scale σ_λ and $\sigma_{\vec{x}}$,

$$\hat{E}(\lambda,\vec{x}) = \hat{E} + \begin{pmatrix}\vec{x}\\ \lambda\end{pmatrix}^T \begin{bmatrix}\hat{E}_{\vec{x}}\\ \hat{E}_\lambda\end{bmatrix} + \frac{1}{2}\begin{pmatrix}\vec{x}\\ \lambda\end{pmatrix}^T \begin{bmatrix}\hat{E}_{\vec{x}\vec{x}} & \hat{E}_{\vec{x}\lambda}\\ \hat{E}_{\lambda\vec{x}} & \hat{E}_{\lambda\lambda}\end{bmatrix}\begin{pmatrix}\vec{x}\\ \lambda\end{pmatrix} + \dots \tag{27}$$

The mth differentiation with respect to λ and the nth differentiation with respect to $\vec{x}$ may be transported using Gaussian derivative filters in the well-known N-jet [27]:

$$\hat{E}_{\lambda^m\vec{x}^n}(\lambda,\vec{x}) = E(\lambda,\vec{x}) * G_{\lambda^m\vec{x}^n}(\lambda,\vec{x};\sigma_\lambda,\sigma_{\vec{x}}). \tag{24}$$

Here, $G_{\lambda^m\vec{x}^n}(\lambda,\vec{x};\sigma_\lambda,\sigma_{\vec{x}})$ are the Gaussian-shaped spatio-spectral probes or color receptive fields. The coefficients of the Taylor expansion of $\hat{E}(\lambda,\vec{x})$ together form a complete representation of the local image structure. Truncation of the Taylor expansion results in an approximate representation, optimal in least-squares sense.

It appears that the above Gaussian color model approximates the Hering basis [28] for human color vision when truncated at second order and taking the parameters $\lambda_0 \simeq 520$ nm and $\sigma_\lambda \simeq 55$ nm [17]. We follow this case and denote spectral differential quotients by $\hat{E}$, $\hat{E}_\lambda$, and $\hat{E}_{\lambda\lambda}$, and spatial differential quotients by $\hat{E}_x$, $\hat{E}_{\lambda x}$, and $\hat{E}_{\lambda\lambda x}$.

4.2 The Gaussian Color Model by a RGB-Camera

Spectral differential quotients are obtained by a linear combination of given (RGB) sensitivities, whereas spatial differential quotients are obtained by convolution with Gaussian derivative filters. When establishing the Gaussian color model for a RGB-camera, we note following [17] that the first three components $\hat{E}$, $\hat{E}_\lambda$, and $\hat{E}_{\lambda\lambda}$ of the Gaussian color model very well approximate the CIE 1964 XYZ basis when taking $\lambda_0 = 520$ nm and $\sigma_\lambda = 55$ nm. A camera is developed to capture the same color space as humans, hence we assume the RGB-sensitivities to span a similar spectral bandwidth and to have a similar central wavelength. When camera response is linearized, a RGB-camera approximates the CIE 1964 XYZ basis for colorimetry by the linear transform [29]

$$\begin{bmatrix}\hat{X}\\ \hat{Y}\\ \hat{Z}\end{bmatrix} = \begin{pmatrix}0.62 & 0.11 & 0.19\\ 0.3 & 0.56 & 0.05\\ -0.01 & 0.03 & 1.11\end{pmatrix}\begin{bmatrix}R\\ G\\ B\end{bmatrix}. \tag{29}$$

The best linear transform from XYZ values to the Gaussian color model is given by [17]

$$\begin{bmatrix}\hat{E}\\ \hat{E}_\lambda\\ \hat{E}_{\lambda\lambda}\end{bmatrix} = \begin{pmatrix}-0.48 & 1.2 & 0.28\\ 0.48 & 0 & -0.4\\ 1.18 & -1.3 & 0\end{pmatrix}\begin{bmatrix}\hat{X}\\ \hat{Y}\\ \hat{Z}\end{bmatrix}. \tag{30}$$

The product of (29) and (30) gives the desired implementation of the Gaussian color model in RGB terms,

$$\begin{bmatrix}\hat{E}\\ \hat{E}_\lambda\\ \hat{E}_{\lambda\lambda}\end{bmatrix} = \begin{pmatrix}0.06 & 0.63 & 0.27\\ 0.3 & 0.04 & -0.35\\ 0.34 & -0.6 & 0.17\end{pmatrix}\begin{bmatrix}R\\ G\\ B\end{bmatrix}. \tag{31}$$

Note that we try to achieve derivative filters in the spectral domain by transforming the spectral responses as given by the RGB-filters. The transformed filters may be imperfect, but are likely to offer accurate estimates of differential measurements. When the spectral responses of

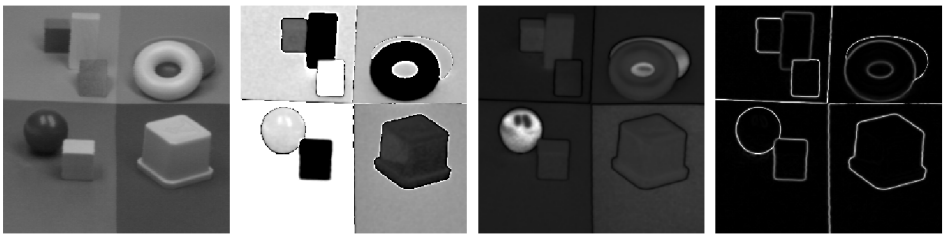

Fig. 2. Example of the invariants associated with $\hat{H}$. The example image is shown left, then $\hat{H}$, the derived expression $\hat{S}$, and gradient magnitude $\hat{H}_w$. Intensity changes and highlights are suppressed in the $\hat{H}$ and $\hat{H}_w$ image. The $\hat{S}$ image shows a low purity at color borders, due to mixing of colors on two sides of the border. For all pictures, $\sigma_{\vec{x}} = 1$ pixel and the image size is 256×256.

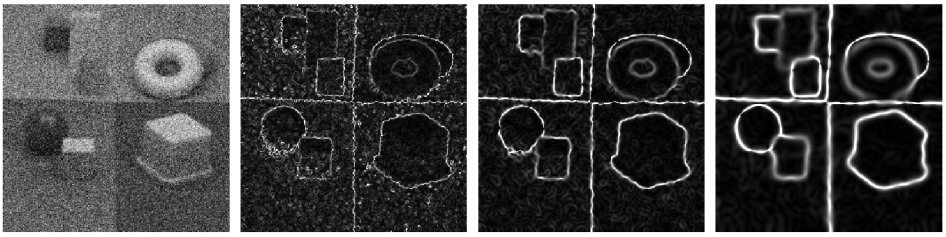

Fig. 3. The influence of white additive noise on gradient magnitude $\hat{H}_w$. Independent Gaussian zero-mean noise is added to each of the RGB channels, SNR = 5, and $\hat{H}_w$ is determined for $\sigma_{\vec{x}} = 1$, $\sigma_{\vec{x}} = 2$ and $\sigma_{\vec{x}} = 4$ pixels, respectively. Note the noise robustness of the hue gradient $\hat{H}_w$ for larger $\sigma_{\vec{x}}$.

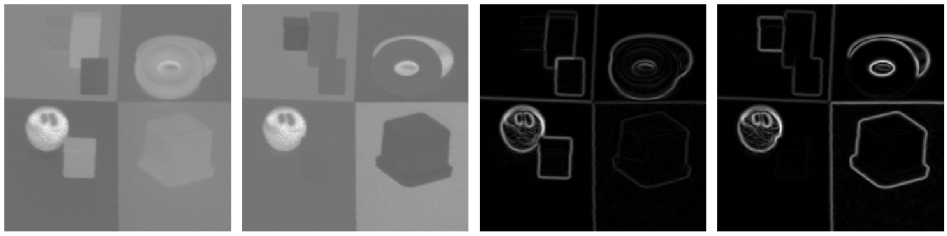

Fig. 4. Examples of the normalized colors $\hat{C}_\lambda$ denoting the first spectral derivative, $\hat{C}_{\lambda\lambda}$ denoting the second spectral derivative, and their gradient magnitudes $\hat{C}_{\lambda w}$ and $\hat{C}_{\lambda\lambda w}$, respectively. Note that intensity edges are being suppressed, whereas highlights are still present.

the RGB-filters are known, a better transform can be obtained.

4.3 Measurement of Geometrical Color Invariants

Measurement of the geometrical color invariants is obtained by substitution of (31) in the invariant expressions derived in Section 3. Measured values for the geometrical color invariants given in Tables 2 and 4 are obtained by substitution of E, E_λ, and $E_{\lambda\lambda}$ for the measured values $\hat{E}$, $\hat{E}_\lambda$, and $\hat{E}_{\lambda\lambda}$ at given scale $\sigma_{\vec{x}}$. In this section, we demonstrate the color invariant properties for each of the assumed imaging conditions by applying the invariants for an example image. The invariants regarding a uniform object are not demonstrated separately, since the expressions are included in the invariants for colored illumination.

From here on, we make two assumptions regarding an equal energy spectrum. We assume that the equal energy spectrum is approximated by a common light source (TL, incandescent, or daylight), and that the camera is correctly white-balanced to the light source. Most light sources yield broad-band emission spectra. Hence, the spectral components of the white-balanced light source are approximately constant over the wavelengths with respect to the integration scale of the camera. Equal energy illumination is now referred to as white light.

4.3.1 Measurement of Invariants for White Illumination

The invariant $\hat{H}$ is representative for hue or dominant color of the material, disregarding intensity and highlights. The pseudoinvariant $\hat{S}$ (10) denotes the purity of the color and, therefore, is sensitive to highlights since at these points color is desaturated. An example is shown in Fig. 2. The invariant $\hat{H}_w$ represents the hue gradient magnitude, detecting color edges independent of intensity and highlights, as demonstrated in Fig. 2.

Common expressions for hue are known to be noise sensitive. In the scale frame, Gaussian regularization offers a trade-off between noise and detail sensitivity. The influence of noise on hue gradient magnitude $\hat{H}_w$ for various $\sigma_{\vec{x}}$ is shown in Fig. 3. The influence of noise on the hue edge detection is drastically reduced for larger observational scale $\sigma_{\vec{x}}$.

4.3.2 Measurement of Invariants for White Illumination and Matte, Dull Surfaces

The invariants $\hat{C}_\lambda$ and $\hat{C}_{\lambda\lambda}$ represent normalized color, consequently their spatial derivatives measure the normalized color gradients. $\hat{C}_{\lambda w}$ may be interpreted as the color gradient magnitude for transitions in first order spectral derivative, whereas $\hat{C}_{\lambda\lambda w}$ detects edges related to the second order spectral derivative. An example of the normalized colors and its gradients are shown in Fig. 4.

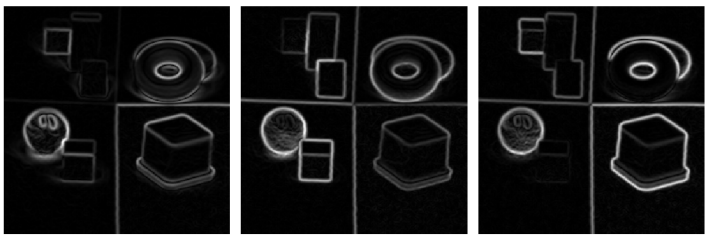

Fig. 5. Examples of the gradient magnitudes $\hat{I}_w$, $\hat{W}_{\lambda w}$, and $\hat{W}_{\lambda\lambda w}$, respectively. Note all images show edges due to intensity differences and highlights. $\hat{I}_w$ shows purely intensity edges or shadow edges, while $\hat{W}_{\lambda w}$ and $\hat{W}_{\lambda\lambda w}$ show color edges.

4.3.3 Measurement of Invariants for White and Uniform Illumination, and Matte, Dull Surfaces, and Planar Objects

The invariant $\hat{I}_w$ denotes intensity or shadow edges, whereas the invariants $\hat{W}_{\lambda w}$ and $\hat{W}_{\lambda\lambda w}$ represent color edges. $\hat{W}_{\lambda w}$ may be interpreted as the gradient magnitude for the first spectral derivative. A similar interpretation holds for $\hat{W}_{\lambda\lambda w}$, but here edges caused by the second spectral derivative are detected. An example of the gradients is shown in Fig. 5.

4.3.4 Measurement of Invariants for Colored Illumination

The invariant $\hat{N}_{\lambda w}$ and $\hat{N}_{\lambda ww}$ may be interpreted as the reflectance function gradient magnitudes for spectral first and second order derivatives, respectively. Hence, material edges are detected independent of illumination intensity and illumination color. An example of the gradients $\hat{N}_{\lambda w}$ and $\hat{N}_{\lambda\lambda w}$ is shown in Fig. 6. In [19], the authors investigate the illumination color invariance of the proposed edge strength, resulting in a significant reduction of chromatic variation due to illumination color. For a more elaborate discussion on the subject, which is beyond the scope of this paper, we refer to [19].

4.3.5 Total Color Gradients

The expressions for total gradient magnitude are given by $\hat{E}_w$, $\hat{W}_w$, $\hat{C}_w$, $\hat{N}_w$, and $\hat{H}_w$. The proposed edge strength measures may be ordered by degree of invariance, yielding $\hat{E}_w$ as measure of spectral edge strength, $\hat{W}_w$ as measure of color edge strength, disregarding intensity level, $\hat{C}_w$ as measure of chromatic edge strength, disregarding intensity distribution, $\hat{N}_w$ as measure of chromatic edge strength, disregarding illumination, and $\hat{H}_w$ as measure of dominant wavelength, disregarding intensity and highlights. An example of the proposed measures is shown in Fig. 7.

4.4 Discriminative Power for RGB Recording

In order to investigate the discriminative power of the proposed invariants, edge detection between 1,013 different colors of the PANTONE[1] color system is examined. The PANTONE colors span a convex, nontriangular set in chromaticity space, hence may be considered as the mixture of various inks. The set is representative for natural surface reflection spectra since most reflection functions may be modeled by a linear five to seven parameter model [30]. The colors are uniformly distributed in color space. The 1,013 PANTONE colors[2] are recorded by a RGB-camera (Sony DXC-930P), under a 5200K daylight simulator (Little Light, Grigull, Jungingen, Germany). Purely achromatic patches are removed from the data set, leaving 1,000 colored patches. In this way, numerically unstable results for set $\hat{H}$ are avoided.

Color edges are formed by combining each of the patches with all others, yielding 499,500 different edges. Edges are defined virtually by computing the left-hand part on one patch and the right-hand side of the filter on one of the other patches. The total edge strength measures for invariants $\hat{E}$, $\hat{W}$, $\hat{C}$, $\hat{N}$, and $\hat{H}$ (Table 3) are measured for each color combination at a scale of $\sigma_x = \{0.75, 1, 2, 3\}$ pixels, hence evaluating the total performance of each set of invariants. Discrimination between colors is determined by evaluating the ratio of discriminatory contrast between patches to within patch noise,

$$DNR_c(i,j) = \frac{\hat{c}_{ij}}{\max_k \sqrt{\frac{1}{N^2}\sum_{x,y} \hat{c}_k(x,y)^2}}, \tag{32}$$

where $\hat{c}$ denotes one of the edge strength measures for $\hat{E}$, $\hat{W}$, $\hat{C}$, $\hat{N}$, or $\hat{H}$, respectively. Further, $\hat{c}_{ij}$ denotes the edge strength between patch i and j, and $\hat{c}_k$ denotes the responses of the edge detector to noise within patch k. Hence, for detector $\hat{c}$, the denominator in expression (32) expresses the maximum response over the 1,000 patches due to noise, whereas the numerator expresses the response due to the color edge. Two colors are defined to be discriminable when $DNR \geq 3$, effectuating a conservative threshold.

The results of the experiment are shown in Table 6. For a spatial scale $\sigma_x = 3$, an accurate estimate of color value is obtained. Hence, the trichromatic invariants $\hat{E}$ and $\hat{W}$ are able to distinguish between all of the PANTONE colors. This is not surprising, since the colors are made to look different. However, for the dichromatic invariants $\hat{C}$ and $\hat{N}$ intensity is removed. For these invariants, no distinction can

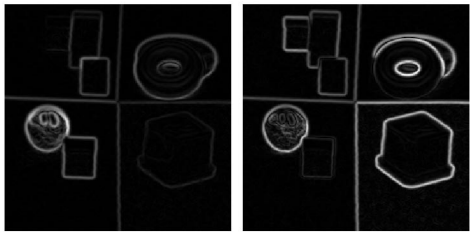

Fig. 6. Examples of the gradient magnitudes $\hat{N}_{\lambda w}$ (left) and $\hat{N}_{\lambda\lambda w}$. Note that intensity edges are suppressed. Further, note that the assumptions underlying this invariant does not account for highlights and interreflections, as is seen in the figure.

1. PANTONE is a trademark of Pantone, Inc.
2. We use the PANTONE edition 1992-1993, Groupe BASF, Paris, France.

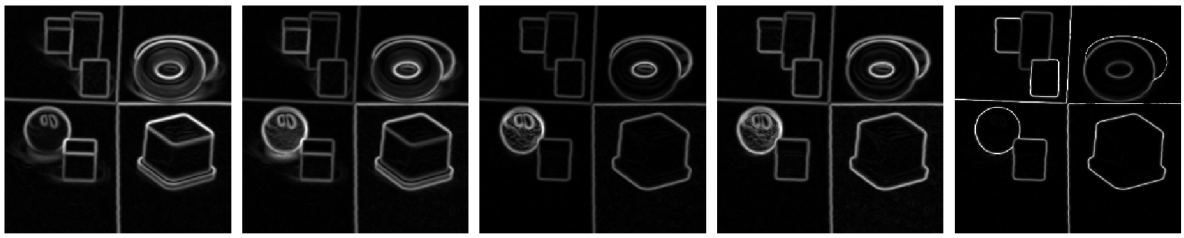

Fig. 7. Examples for the total color edge strength measures. Shown is $\hat{E}_w$ which is not invariant, then $\hat{W}_w$ invariant for a constant gain or intensity factor. Note that these images show intensity, color, and highlight boundaries. Further, $\hat{C}_w$ and $\hat{N}_w$ invariant for shading are shown. Finally, $\hat{H}_w$ invariant for shading and highlights. The effect of intensity and highlights on the different invariants are in accordance with Table 1.

be made between colors similar in chromaticity. Evaluation of the PANTONE colors show that for each color, there are on average 10 colors which only differ in intensity, thus 990 left to be distinguished. For these invariants, the resulting discrimination of 970 different colors is close to optimal. For the unichromatic invariant $\hat{H}$, only the dominant wavelenth of the measured spectrum is considered. To investigate invariance, we may subdivide all colors in the categories {red, yellow, green, blue, purple}. Following a similar argumentation as for the intensity invariants, we may state that e.g. all green colors can not be distinguished from each other. Then, given the rough categorization, 200 out of 1,000 colors are similar, leaving 800 to be distinguished. The result obtained, discriminating between 460 colors, is not optimal due to instability of (9) for desaturated colors.

When the spatial scale σ_x decreases, discrimination degrades. A larger spatial scale yields better reduction of noise, hence a more accurate estimate of the true color is obtained. The results shown for $\sigma_x \geq 2$ are saturated for $\hat{E}$ and $\hat{W}$. Hence, a larger set of colors can be discriminated than shown here. Note also that the power of discrimination expressed as the amount of discriminable colors is inversely proportional to the degree of invariance. These are very encouraging results given a standard RGB-camera and not a spectrophotometer. To discriminate 450 to 950 colors while calculating invariance on just two patches in the image is helpful for many practical image retrieval problems.

5 Conclusion

In this paper, we have derived geometrical color invariant expressions describing material properties under three independent assumptions regarding the imaging conditions, 1) white or colored illumination, 2) matte, dull object or general object, or 3) uniformly stained object or generally colored object. The reflectance model under which the invariants remain valid is useful for a wide range of materials [21]. Furthermore, we have established the robust measurement of object reflectance from RGB-images, based on the Gaussian scale-space paradigm. Experiments on an example image showed the invariant set $\hat{C}$ and $\hat{N}$ to be successful in disregarding shadow edges, whereas the set $\hat{H}$ is shown to be successful in discounting both shadow edges and highlights. In [19], the authors have investigated the degree of illumination color invariance for set $\hat{N}$.

We showed the discriminative power of the invariants to be orderable by broadness of invariance. Highest discriminative power is obtained by set $\hat{W}$ which has the tightest set of disturbing conditions, namely overall illumination intensity or camera gain. Discrimination degraded for set $\hat{C}$ and $\hat{N}$, invariant for shading effects and illumination color. Set $\hat{H}$, invariant for shadows and highlights, has lowest discriminative power. Illumination and viewing direction invariance is evaluated in [31] by experiments on a collection of real-world surfaces. Discriminating power is increased when considering a larger spatial scale σ_x. Hence, a larger spatial scale results in a more accurate estimate of color at the point of interest, increasing the accuracy of the result. The aim of the paper is reached in that high color discrimination resolution is achieved while maintaining constancy against disturbing imaging conditions, both theoretically as well as experimentally.

We have restricted ourselves in several ways. We have derived expressions up to the second spatial order, and investigated their performance only for the spatial gradient. The derivation of higher order derivatives is straightforward, and may aim in corner detection [9]. Usually many derivatives are involved here, raising some doubt on the sustainable accuracy of the result. Consequently, a larger spatial scale may be necessary to increase the accuracy of measurements involving higher order derivatives. Further, we have only considered spectral derivatives up to second order, yielding compatibility with human color vision. For a spectrophotometer, measurements can be obtained at different positions λ_0, for different scales σ_λ, and for higher spectral differential order, thereby exploiting the generality of the Gaussian color model.

TABLE 6
Discriminative Power

	$\sigma_x = 0.75$	$\sigma_x = 1$	$\sigma_x = 2$	$\sigma_x = 3$
$\hat{E}$	970	983	1000	1000
$\hat{W}$	944	978	1000	1000
$\hat{C}$	702	820	949	970
$\hat{N}$	631	757	962	974
$\hat{H}$	436	461	452	462

For each Invariant, the mumber of colors is given which can be discriminated from one another in the PANTONE color system (1,000 colors). The number refers to the amount of colors still to be distinguished with the conservative criterion $DNR \geq 3$ given the hardware and spatial scale σ_x. For $\sigma_x \geq 2$, $\hat{E}$ and $\hat{W}$ discriminate between all patches, hence, the results are saturated.

We provided different classes of color invariants, under general assumptions regarding the imaging conditions. We have shown how to reliably measure color invariants from RGB images by using the Gaussian color model. The Gaussian color model extents the differential geometry approaches from gray-value images to multispectral differential geometry. Further, we experimentally proved the color invariants to be successful in discounting shadows and highlights, resulting in accurate measurements of surface reflectance properties. The presented framework for color measurement is well-defined on a physical basis, hence it is theoretically better founded as well as experimentally better evaluated than existing methods for the measurement of color features in RGB-images.

ACKNOWLEDGMENTS

The authors are grateful to Theo Gevers for advice and suggestions and for supplying the example figure (Fig. 2a). The authors thank Frans Cornelissen for helpful suggestions.

REFERENCES

[1] R. Gershon, D. Jepson, and J.K. Tsotsos, "Ambient Illumination and the Determination of Material Changes," *J. Optical Soc. Am. A,* vol. 3, pp. 1700-1707, 1986.
[2] T. Gevers and A.W.M. Smeulders, "Color Based Object Recognition," *Pattern Recognition,* vol. 32, pp. 453-464, 1999.
[3] G. Healey and A. Jain, "Retrieving Multispectral Satellite Images Using Physics-Based Invariant Representations," *IEEE Trans. Pattern Analysis and Machine Intelligence,* vol. 18, pp. 842-848, 1996.
[4] S.A. Shafer, "Using Color to Separate Reflection Components," *Color Resolution Applications,* vol. 10, no. 4, pp. 210-218, 1985.
[5] E. Angelopoulou, S. Lee, and R. Bajcsy, "Spectral Gradient: A Material Descriptor Invariant to Geometry and Incident Illumination," *Proc. Seventh IEEE Int'l Conf. Computer Vision,* pp. 861-867, 1999.
[6] H. Stokman and T. Gevers, "Detection and Classification of Hyper-Spectral Edges," *Proc. 10th British Machine Vision Conf.,* pp. 643-651, 1999.
[7] L.M.J. Florack, B.M. ter Haar Romeny, J.J. Koenderink, and M.A. Viergever, "Cartesian Differential Invariants in Scale-Space," *J. Math. Imaging Vision,* vol. 3, no. 4, pp. 327-348, 1993.
[8] T. Lindeberg, *Scale-Space Theory in Computer Vision.* Boston: Kluwer Academic, 1994.
[9] *Geometry-Driven Diffusion in Computer Vision.* B.M. ter Haar Romeny, ed., Boston: Kluwer Academic, 1994.
[10] J.J. Koenderink, "The Structure of Images," *Biological Cybernetics.* vol. 50, pp. 363-370, 1984.
[11] J.J. Koenderink and A.J. van Doorn, "Receptive Field Families," *Biological Cybernetics,* vol. 63, pp. 291-297, 1990.
[12] T. Gevers, S. Ghebreab, and A.W.M. Smeulders, "Color Invariant Snakes," *Proc. Ninth British Machine Vision Conf.,* P.H. Lewis and M.S. Nixon, eds., pp. 659-670, 1998.
[13] G. Sapiro and D.L. Ringach, "Anisotropic Diffusion of Multivalued Images with Applications to Color Filtering," *IEEE Trans. Image Processing,* vol. 5, no. 11, pp. 1582-1586, 1996.
[14] S. Di Zenzo, "A Note on the Gradient of a Multi-Image," *Computer Vision Graphics Image Processing,* vol. 33, pp. 116-125, 1986.
[15] A. Cumani, "Edge Detection in Multispectral Images," *CVGIP: Graphical Models and Image Processing,* vol. 53, no. 1, pp. 40-51, 1991.
[16] J.J. Koenderink and A. Kappers, *Color Space.* The Netherlands: Utrecht Univ., 1998.
[17] J.M. Geusebroek, R. van den Boomgaard, A.W.M. Smeulders, and A. Dev, "Color and Scale: The Spatial Structure of Color Images," *Proc. Sixth European Conf. Computer Vision,* vol. 1, pp. 331-341, 2000.
[18] J.M. Geusebroek, A. Dev, R. van den Boomgaard, A.W.M. Smeulders, F. Cornelissen, and H. Geerts, "Color Invariant Edge Detection," *Scale-Space Theories in Computer Vision,* pp. 459-464, 1999.
[19] J.M. Geusebroek, "Color and Geometrical Structure in Images" PhD thesis, Univ. of Amsterdam, 2000.
[20] P. Kubelka and F. Munk, "Ein Beitrag zur Optik der Farbanstriche," *Z. Techn. Physik,* vol. 12, p. 593, 1931.
[21] D.B. Judd and G. Wyszecki, *Color in Business, Science, and Industry.* New York: Wiley, 1975.
[22] G. Wyszecki and W.S. Stiles, *Color Science: Concepts and Methods, Quantitative Data and Formulae.* New York: Wiley, 1982.
[23] G. Healey, "Using Color for Geometry-Insensitive Segmentation," *J. Optical Soc. Am. A,* vol. 6, pp. 920-937, 1989.
[24] P. Kubelka, "New Contribution to the Optics of Intensely Light-Scattering Materials, part I," *J. Optical Soc. Am.,* vol. 38, no. 5, pp. 448-457, 1948.
[25] P. Olver, G. Sapiro, and A. Tannenbaum, "Differential Invariant Signatures and Flows in Computer Vision: Asymmetry Group Approach," *Geometry-Driven Diffusion in Computer Vision.* B.M. ter Haar Romeny, ed., Boston: Kluwer Academic, 1994.
[26] T. Gevers and H. Stokman, "Reflectance Based Edge Classification," *Proc. Vision Interface,* pp. 25-32, 1999.
[27] L.M.J. Florack, B.M. ter Haar Romeny, J.J. Koenderink, and M.A. Viergever, "Scale and the Differential Structure of Images," *Image and Vision Computing,* vol. 10, no. 6, pp. 376-388, 1992.
[28] E. Hering, *Outlines of a Theory of the Light Sense.* Cambridge, Mass.: Harvard Univ. Press, 1964.
[29] "Basic Parameter Values for the (HDTV) Standard for the Studio and for International Programme Exchange,"Technical Report ITU-R Rec. BT. 709, Switzerland, 1990.
[30] L.T. Maloney, "Evaluation of Linear Models of Surface Spectral Refelctance with Small Number of Parameters," *J. Optical Soc. Am. A,* vol. 3, pp. 1673-1683, 1986.
[31] J.M. Geusebroek, A.W.M. Smeulders, and R. van den Boomgaard, "Measurement of Color Invariants," *Proc. IEEE Conf. Computer Vision and Pattern Recognition,* vol. 1, pp. 50-57, 2000.

Jan-Mark Geusebroek received the PhD degree in computer sciences from the University of Amsterdam in 2000. He is a postdoctoral fellow in the Intelligent Sensory Information Systems (ISIS) group at the University of Amsterdam. His research interests are in front-end vision, especially color and texture vision. His current research concentrates on material recognition for retrieval from large image collections.

Rein van den Boomgaard graduated from the Delft University in 1988 and received the PhD degree from the University of Amsterdam in 1992. He is an assistant professor in the Intelligent Sensory Information Systems (ISIS) group at the University of Amsterdam. He is working in the field of computer vision and image processing with research interests in color vision, scale-space theory, and mathematical morphology. He is now working towards a computational theory of "image processing without pixels." He is a member of the IEEE Computer Society.

Arnold W.M. Smeulders is a full professor in multimedia information analysis with a special interest in content-based image retrieval systems, as well as, systems for the analysis of video. He is the director of the Informatics Research Institute at the University of Amsterdam. He heads the ISIS research group of 25 persons which concentrate on theory, practice, and implementation of image retrieval and computer vision. The group has an extensive record in co-operations with Dutch industry in the area of multimedia and video analysis. Until recently, he was the associate editor of *IEEE Transactions on Pattern Analysis and Machine Intelligence*. He received a Fulbright grant at Yale University in 1987, and a visiting professorship at the City University Hong Kong in 1996, and ETL Tsukuba Japan in 1998. He was elected a fellow of the International Association of Pattern Recognition. His current research interest is in image retrieval, especially perceptual similarity, material recognition, and the connection between pictures and language. He is a senior member of the IEEE.

Hugo Geerts received the PhD in biophysics in the study of protein-protein and protein-lipid interaction at the University of Antwerp in 1984. In parallel, he also received the Bachelor in Medicine degree. He joined Janssen Pharmaceutica in the Department of Cell Biology where advanced microscopic techniques were developed, together with the appropriate image analysis techniques. In 1991, he switched to studying the cytoskeletal aspects of neurodegeneration, especially in Alzheimer's disease (the group of Neurobiology). At the same time, (given his background mix of physics and medicine) he set up a group of quantitative morphology with the aim of developing medium-throughput morphological screening systems (High-Content screening). He has coauthored more than 75 papers and seven patents.